THE ASTROPHYSICAL JOURNAL, 430:601–609, 1994 August 1

SOFT X-RAY AND H I SURVEYS OF THE LOW N_H REGION IN URSA MAJOR

S. L. SNOWDEN[1,2,3] AND G. HASINGER
Max-Planck-Institut für Extraterrestrische Physik, D-8046 Garching, Germany
K. JAHODA
Laboratory for High Energy Astrophysics, NASA/Goddard Space Flight Center, Greenbelt, MD 20771
FELIX J. LOCKMAN
National Radio Astronomy Observatory,[4] P.O. Box 2, Green Bank, WV 24944
AND
D. MCCAMMON AND W. T. SANDERS
Department of Physics, University of Wisconsin—Madison, 1150 University Avenue, Madison, WI 53706
Received 1993 May 24; accepted 1994 January 28

ABSTRACT

A region of almost 300 deg^2 in Ursa Major around the direction of the lowest neutral hydrogen column density in the sky has been surveyed in the $\frac{1}{4}$ keV X-ray band ($\sim$0.12–0.284 keV at 10% of the peak response) using the *ROSAT* PSPC and has been fully mapped in the 21 cm line of neutral hydrogen with an angular resolution of 21′ or better. We present maps of these two data sets and an analysis of the spatial correlation between them. Over the entire field, the $\frac{1}{4}$ keV band X-ray count rate shows a strong negative correlation with the column density of Galactic neutral hydrogen. We discuss the local, extragalactic, and halo contributions to the observed diffuse X-ray intensity and derive an upper limit to the Galactic X-ray emission originating beyond this H I distribution that is more than a factor of 7 smaller than the inferred flux beyond the Draco nebula, an apparent halo object located $\sim$41° away. This implies that while there may be significant amounts of hot gas in the Galactic halo, its properties must vary strongly across the sky.

Subject headings: Galaxy: halo — radio lines: ISM — X-rays: interstellar

1. INTRODUCTION

There is a distinguished history of speculation about the existence of hot ($\sim 10^6$ K) X-ray–emitting gas in the halo far above the Galactic plane (Spitzer 1956; Shapiro & Field 1976; Chevalier & Oegerle 1979; Bregman 1980; Marshall & Clark 1984; Hirth, Mebold, & Müller 1985; Edgar & Chevalier 1986; Raymond 1992). Observations of the $\frac{1}{4}$ keV band diffuse X-ray background, however, have always been consistent with a model in which essentially all of the detected emission originates within 100–200 pc of the Sun (the data and arguments are summarized in McCammon & Sanders 1990). In particular, observations in some key directions appear to rule out any substantial contribution to the soft X-ray background from an isotropic $\frac{1}{4}$ keV band component arising beyond the Galactic H I layer (McCammon et al. 1976; Burrows et al. 1984).

One of the most intriguing recent developments in X-ray astronomy, therefore, has been the detection by the *Röntgen Satellite* (*ROSAT*) of shadows in the $\frac{1}{4}$ keV X-ray background toward high-latitude interstellar clouds in Draco. The data imply that only about half of the emission seen toward those clouds arise from the foreground (local) region, while the rest must originate beyond the clouds (Burrows & Mendenhall 1991; Snowden et al. 1991). The distance to the absorbing gas in the Draco complex is not known with great certainty, but optical spectroscopy (Lilienthal et al. 1991) indicates that it is >200 pc above the Galactic plane. These new observations can be reconciled with previous data only if the "halo" emission which provides half of the flux in Draco is much less in several other directions where similar measurements have been made (McCammon et al. 1976; Burrows et al. 1984). Patchy halo emission might explain the $\frac{1}{4}$ keV enhancements observed at high latitudes, but the difficulty remains that these enhancements are just as bright at even lower energies, where absorption by the observed H I should be very large.

In this paper, we analyze the correlations between the *ROSAT* $\frac{1}{4}$ keV band sky survey data and 21 cm H I data from a high-latitude region where the column density of Galactic neutral hydrogen is well determined and unusually small. This region contains two intermediate negative velocity clouds whose distances are not yet known, but whose peculiar velocity suggests a similarity to the Draco complex. These clouds also shadow a substantial fraction of the observed $\frac{1}{4}$ keV X-ray flux. The upper limit we derive for the X-ray intensity originating beyond the Galactic neutral hydrogen in this field, however, is substantially smaller than the intensity implied to arise behind the Draco clouds.

2. THE DATA

2.1. H I *Data*

The 21 cm H I data used here are from Lockman, Jahoda, & McCammon (1986), Jahoda, Lockman, & McCammon (1990), and new observations made in 1988, 1989, and 1990 on the 43 m telescope of the National Radio Astronomy Observatory (NRAO) in Green Bank, West Virginia. The spectra were

[1] Also Department of Physics, University of Wisconsin—Madison, 1150 University Avenue, Madison, WI 53706.
[2] Also Laboratory for High Energy Astrophysics, NASA/Goddard Space Flight Center, Greenbelt, MD 20771.
[3] Also Universities Space Research Association.
[4] The National Radio Astronomy Observatory is operated by Associated Universities, Inc., under a cooperative agreement with the National Science Foundation.

reduced and corrected for stray radiation using procedures described by Lockman et al. (1986) and Jahoda et al. (1990), which involve bootstrapping Green Bank observations to the Bell Labs H I survey (Stark et al. 1992). In all, the H I data set consists of about 12,000 spectra taken with the NRAO 43 m telescope on a 10′ × 10′ grid at an angular resolution of 21′, and ~2000 spectra from the NRAO 91 m telescope taken on a 2.′7 × 5′ grid with 11′ angular resolution that cover the lowest column density region of Ursa Major. The H I data extend from about 10^h to $12^h.3$ right ascension and from 51° to 67° in declination (1950). For comparison with the *ROSAT* data, the H I maps were interpolated and recast into an equal-area polar projection centered on $(\alpha, \delta)_{2000} = (11^h, 60°)$ with 3.′2 × 3.′2 pixels.

The experimental errors in the H I observations vary over the region because the lowest N_H areas were observed for a longer time than other positions. Moreover, baseline uncertainties and effects introduced by the stray radiation correction procedure add errors that are not easily quantified. Jahoda et al. (1990) estimated that the systematic uncertainty in the total column density of any spectrum over the inner parts of the region is typically 0.5×10^{19} cm^{-2}, but might be twice this in some areas.

2.2. *X-Ray Data*

The X-ray data used in this paper were collected with the Position Sensitive Proportional Counter (PSPC; Pfeffermann et al. 1987) on the *ROSAT* (Trümper 1983) X-ray Telescope (XRT; Aschenbach 1988) during the *ROSAT* all-sky survey (Snowden & Schmitt 1990; Voges 1992; Snowden et al. 1994a) between 1990 October 13 and 1990 November 21. During the survey, the sky was scanned along a great circle that passed through both ecliptic poles and whose ecliptic longitude changed by ~4′ from orbit to orbit. At the ~50° ecliptic latitude of the Ursa Major region, a given point on the sky was within the 2° field of view of the PSPC on every orbit for nearly 3 days. The cumulative vignetting-corrected exposure for a given point in this field is typically 350–700 s.

The data were derived from photon event files and ancillary data provided by the Standard Analysis Software System (SASS; Voges et al. 1992), and were processed in two pulse-height bands: the R1 band (PI channels 8–19, see Snowden et al. 1994b) and the R2 band (channels 20–41). One channel covers ~10 eV. The R1 and R2 band data were combined to produce a $\frac{1}{4}$ keV band data set which is analyzed in this paper. Figure 1 shows the response function for the $\frac{1}{4}$ keV band.

From the survey data, SASS first produced photon event files (PEFs) for strips on the sky of 2° × 360°, which overlapped at the ecliptic poles and whose edges touched in the ecliptic plane. Periods of short-term (one or two orbit) enhancement of the PSPC background were eliminated by comparing the X-ray count rates in 2°, 10°, and 18° segments from successive orbits and excluding time intervals with enhancements that were more than 5 times the statistical count rate uncertainty. For the $\frac{1}{4}$ keV band in this region of the sky, the statistical count rate uncertainty over an 18° segment is ~2%. Since a single scan typically contributes less than 10% of the counts to any part of the field, a single contaminated orbit just below the 5 σ threshold for exclusion could erroneously enhance the count rate from a given direction by at most 1%. About 5% of the total sky-survey exposure of the Ursa Major region is excluded from the $\frac{1}{4}$ keV band data set due to short-term enhancements.

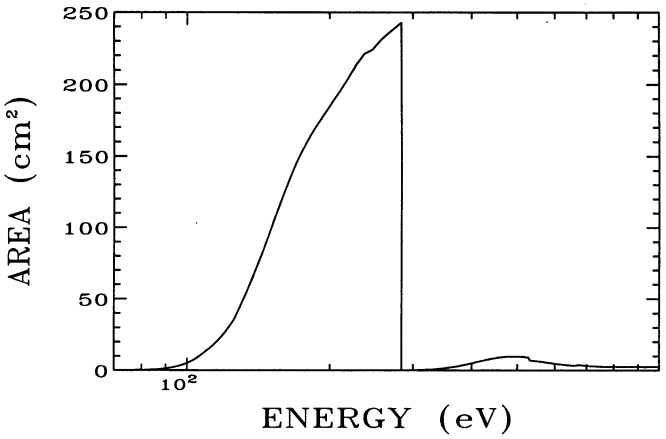

FIG. 1.—*ROSAT* PSPC response function for the $\frac{1}{4}$ keV band (standard bands R1 + R2).

Events remaining in the SASS PEFs were sorted into arrays representing maps of each 2° × 360° strip with 1.′6 × 1.′6 pixels. For the same strips of the sky, ancillary data files were used to create additional arrays that contain the livetime, a point-source mask, and modeled values for the charged particle background, scattered solar X-rays, and "long-term enhancements" of the PSPC noncosmic background. Fairly accurate models exist for predicting the particle background (Snowden et al. 1992; Plucinsky et al. 1993), and scattered solar X-rays (Snowden & Freyberg 1993), but the origin of the long-term enhancements is not yet understood. They appear primarily in the $\frac{1}{4}$ keV band, are approximately uniform around an orbit, last about 20–30 orbits, and have peak intensities occasionally comparable to the cosmic diffuse X-ray background in the $\frac{1}{4}$ keV band. Their rates were determined empirically by using the redundancy of the *ROSAT* survey geometry: over 97% of the PSPC field overlaps from one orbit to the next, and it is thus possible to separate spatial from temporal variations. The average rates in the particle, scattered solar X-ray, and long-term enhancement arrays were respectively about 0.5%, 3%, and 8% of the $\frac{1}{4}$ keV diffuse flux.

We searched for point sources with a simple sliding-box algorithm. The count rate in each 2 × 2 pixel cell (3.′2 × 3.′2, roughly the survey point response function) was compared to the average count rate of the surrounding eight cells. Cells that were brighter than their surroundings by >3.0 times the statistical uncertainty were flagged and masked from the final images. This procedure removed sources down to a limiting flux of about 1.4×10^{-13} ergs cm^{-2} s^{-1} (0.5–2 keV, assuming the average spectrum of the faint sources found in the center of this region by Hasinger et al. 1993). The $\frac{1}{4}$ keV flux from the faintest sources removed is approximately equal to the diffuse background rate in a 3.′2 × 3.′2 cell.

The number of sources removed ranged from 1.8 deg^{-2} in the low N_H parts of the field ($N_{HI} < 0.8 \times 10^{20}$ cm^{-2}) to 0.8 deg^{-2} in the higher N_H regions ($N_{HI} > 1.2 \times 10^{20}$ cm^{-2}). After subtracting the calculated accidental rate of 0.5 deg^{-2}, these figures are in good agreement with the expected number of detections predicted by the log N–log S relation of Hasinger et al. (1993): 1.5 deg^{-2} and 0.3 deg^{-2}, respectively, for the low- and high-N_H areas.

Data from the individual 2° × 360° strips were combined to produce event, exposure, and instrument background maps covering the Ursa Major region. These maps were in turn

combined to produce count-rate and count-rate uncertainty images. The three arrays containing estimates of charged particle events, scattered solar X-ray events, and long-term enhancement events were subtracted from the event array, and the remainder divided by the livetime array to get an estimate of the true X-ray rate for each pixel. The count-rate uncertainty image was taken to be the square root of the event array divided by the livetime array, since the statistical errors introduced by the background subtraction are negligible. The systematic errors in the particle background and the scattered solar X-ray corrections are likely quite small, while those of the long-term enhancement corrections could be significant if their magnitudes are underestimated. For a further discussion, see Snowden et al. (1994a, b).

For the X-ray images and analysis of this paper, the $\frac{1}{4}$ keV count rate arrays were binned into 19.2 × 19.2 pixels on the same projection and center as the H I data. Pixels of this size have statistical uncertainties (σ_R/R) of ~8% for the average $\frac{1}{4}$ keV X-ray count rate of 947 × 10^{-6} counts s^{-1} $arcmin^{-2}$ and a typical exposure of 500 s.

3. GENERAL PROPERTIES OF THE DATA

3.1. H I

The total H I column density over the Ursa Major region is shown in Figure 2 (Plate 31). The contours were derived from the data smoothed with a 22.4 × 22.4 sliding-box filter. The average value of N_H over the field is 1.1 × 10^{20} cm^{-2}. The lowest N_H is 4.4 × 10^{19} cm^{-2} in the direction identified by Jahoda et al. (1990): $(\alpha, \delta)_{2000} = (10^h36^m, 57°4')$, while the highest value is 3.1 × 10^{20} cm^{-2} near $(\alpha, \delta)_{2000} = (11^h50^m, 61°45')$.

Five of the localized neutral hydrogen maxima in the map are identified as clouds in the IRAS 100 μm data, and four have associated CO emission (Heiles et al. 1988; Reach 1993). In all these directions, the column density of H I alone is $\geq 2 \times 10^{20}$ cm^{-2} so the brightest H I clouds should have an opacity $\gtrsim 2$ to background $\frac{1}{4}$ keV X-rays. The clouds can be divided into two groups according to their LSR velocity. The "intermediate-velocity" clouds are all around −45 km s^{-1}, while the "low-velocity" clouds have $V_{LSR} \approx -10$ km s^{-1}. The H I clouds east of right ascension ~11^h15^m in Figure 2 are at intermediate velocity, and those westward of ~11^h15^m are almost entirely at low velocity. Both velocity components are present in the H I concentrations in the southeast and southwest corners of the field. The more broadly distributed noncloud H I is also concentrated in two major features in the velocity spectra: one near zero velocity and the other near −50 km s^{-1}.

There is no reliable distance estimate to any of the clouds, nor to any other gas in this region of Ursa Major. Optical and UV spectroscopy in other parts of the Galaxy suggests that much of the low-velocity gas is fairly local, i.e., within ~200 pc of the Galactic plane, while most of the −25 to −75 km s^{-1} "intermediate negative velocity" gas might be ~500 pc from the plane (Albert 1983; Danly 1989; Lockman 1991; Albert et al. 1993). The Draco nebula complex, which has a similar peculiar velocity (Goerigk et al. 1983; Mebold et al. 1985; Odenwald & Rickard 1987), seems to be located at least 200 pc above the plane (Lilienthal et al. 1991).

3.2. *X-Rays*

The $\frac{1}{4}$ keV X-ray emission over the same ~16° × 18° field mapped in H I is shown in Figure 3 (Plate 32), smoothed for this figure with a 30′ FWHM circular Gaussian filter. The color bar at the bottom of the figure shows the X-ray count rate. The contours indicate H I column density and are the same as those in Figure 2. Across the field shown in Figure 3, the $\frac{1}{4}$ keV X-ray count rate averaged over 1° × 1° cells varies from 665 ± 21 to 1260 ± 27 × 10^{-6} counts s^{-1} $arcmin^{-2}$, with an average rate of 947 × 10^{-6} counts s^{-1} $arcmin^{-2}$. Figure 4 shows contours of the 14 keV band count rate and total H I column density with a Galactic coordinate grid.

3.3. *The Relationship between N_H and I_X*

There is a general anticorrelation between the H I and X-ray intensities that is easily seen in Figure 3. Every major H I feature is associated with a local minimum in the X-ray intensity, I_X. Table 1 gives the locations and the I_X and N_H values averaged over ~1 deg^2 for five of the highest H I column density peaks and five of the highest X-ray intensity peaks. The X-ray brightness at the location of the thickest H I clouds decreases to a minimum of $I_X \sim 700$ counts s^{-1} $arcmin^{-2}$, independent of whether the clouds are intermediate or low

TABLE 1

X-RAY AND N_H FEATURES

Feature	α_{2000}	δ_{2000}	H I Column Density[a] (10^{20} cm^{-2})	$\frac{1}{4}$ keV Count Rate[a] (10^{-6} counts s^{-1} $arcmin^{-2}$)
		N_H Maxima[a]		
1 G135.3+54.5	11^h52^m	61°38′	2.6[b]	705 ± 20
2 G135.5+51.3	11 38	63 52	2.6[b]	665 ± 21
3	09 59	63 41	2.3[c]	698 ± 21
4	12 13	64 41	2.2[b]	835 ± 23
5	12 00	51 17	2.2[c]	730 ± 26
		X-Ray Maxima[a]		
1	10 53	54 52	0.8	1260 ± 27
2	11 48	55 52	0.9	1236 ± 30
3	11 10	51 38	0.9	1211 ± 34
4 H I minimum	10 37	56 59	0.5	1189 ± 26
5	11 36	66 48	0.8	1170 ± 30

[a] Average over 57.6 × 57.6 pixel.
[b] Primarily at $v < -25$ km s^{-1}.
[c] Primarily at $|v| < 25$ km s^{-1}.

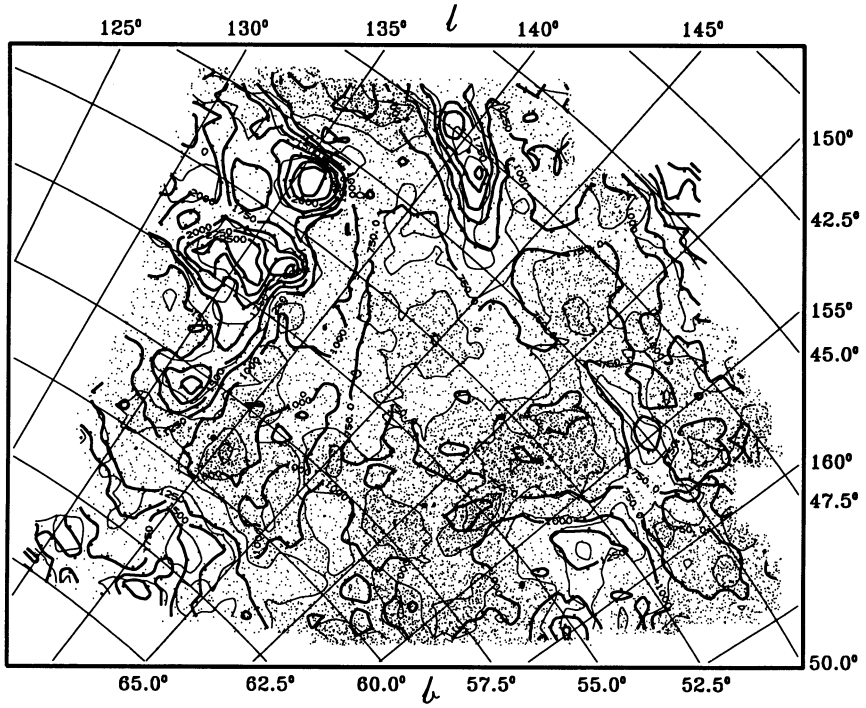

FIG. 4.—Contours of the $\frac{1}{4}$ keV band X-ray brightness from Fig. 3 (*light lines*) with the 21 cm H I contours from Fig. 2 (*heavy lines*) superposed. The shading is darker where the X-ray count rate is higher. Coordinates are Galactic. The H I contour interval is 0.25×10^{20} cm^{-2} from 0.5 to 2.5×10^{20} cm^{-2}. The $\frac{1}{4}$ keV band X-ray contour interval is 100×10^{-6} counts s^{-1} arcmin^{-2} from 800 to 1200×10^{-6} counts s^{-1} arcmin^{-2}.

velocity. The brightest X-ray peaks also seem always to be associated with local minima in $N_{\rm H}$.

As striking as the general anticorrelation between I_X and H I is, however, the correlation shows a large amount of scatter when I_X is plotted against $N_{\rm H}$. Figure 5 shows such a plot for all the data from this field. A close examination of the maps shows two reasons for the large scatter in Figure 5. The first is that the large-scale features in the X-ray intensity are not always exactly coincident with those in the H I. For example, the brightest spot in the X-ray map is near, but not at, the lowest $N_{\rm H}$ location. Again, while the X-ray depression at the top center of the map is mirrored in an H I cloud, the minimum X-ray intensity actually occurs several degrees south of the H I peak. The second reason is that the X-ray intensity shows

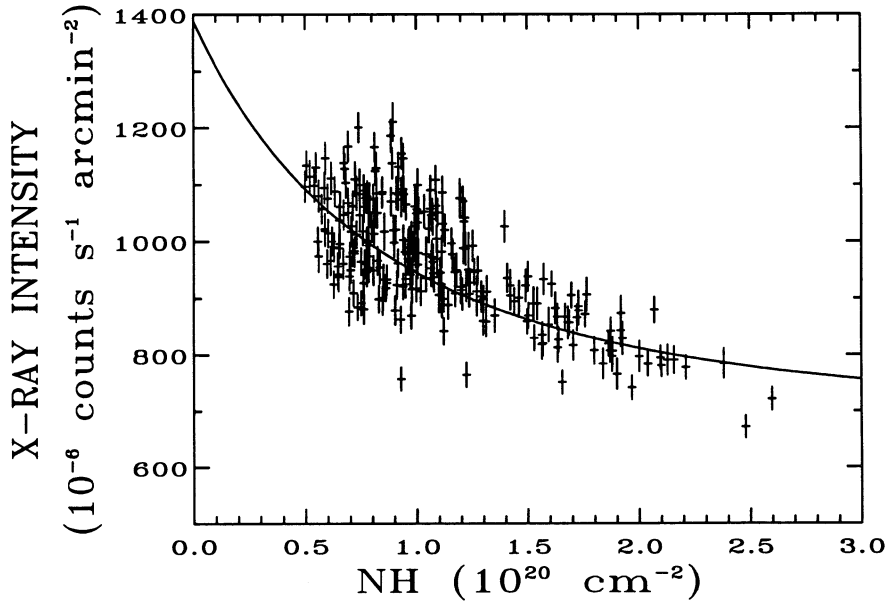

FIG. 5.—Scatter plot of $\frac{1}{4}$ keV band X-ray intensity vs. H I column density for the entire Ursa Major field in $\sim 1° \times 1°$ cells. The solid line is the best-fit two-component absorption model defined by eq. (1).

pixel-to-pixel variations consistently in excess of the expected statistical variations. We tested the assumption that the X-ray intensity is uniform on scales of 1° or less by examining the distribution of χ^2 values obtained from comparing each 19.2 × 19.2 pixel to the average of its eight neighbors. The reduced χ^2 is 1.49 for 2748 degrees of freedom. There is a systematic variation with N_H: pixels with $N_H < 0.8 \times 10^{20}$ cm^{-2} have $\chi^2_\nu = 1.61$ ($\nu = 740$, $\langle I_X \rangle = 1034 \times 10^{-6}$ counts s^{-1} arcmin^{-2}, $\langle \sigma_X \rangle / \langle I_X \rangle = 0.07$), while those with $N_H > 1.2 \times 10^{20}$ cm^{-2} have $\chi^2_\nu = 1.39$ ($\nu = 900$, $\langle I_X \rangle = 863 \times 10^{-6}$ counts s^{-1} arcmin^{-2}, $\langle \sigma_X \rangle / \langle I_X \rangle = 0.08$). Correcting for the small variations in N_H between the central pixel and the average for the surrounding ones reduces these χ^2_ν values only by about 0.03.

We next compared the X-ray intensity in pixels containing clusters of galaxies from the Abell catalog with the average of their eight neighbors. The differences are plotted in Figure 6 as a function of N_H. There is a significant excess on the average ($P < 0.001$) that is concentrated in the pixels with low N_H values. We have corrected the pixel-to-pixel fluctuations for this observed distribution of Abell cluster luminosities ($\Delta\chi^2_\nu = 0.14$ for the low-N_H region and 0.01 for the high-N_H region). Using the log N–log S function and average source spectrum of Hasinger et al. (1993), we find that sources resolved in their deep survey but unresolved in our data contribute 16% of the counts in the low-N_H region and 6% of the counts in the high-N_H region. Their contribution to the excess χ^2_ν is 0.18 and 0.03, respectively, under the assumption of no clustering of the sources. The residual χ^2_ν values are then 1.26 for the low N_H areas and 1.32 for the high N_H. In both regions, about 80% of the remaining excess χ^2 is from pixels with differences exceeding 2.6 σ. In the entire field there are 97 such pixels [$N(> +2.6\sigma) = 40$, $N(< -2.6\sigma) = 57$], while about 26 are expected. They appear to be evenly distributed over the field, except for a 2 σ excess of positive fluctuations in the low-N_H area and a tendency to avoid the central parts of the intermediate-velocity clouds. There is no concentration at the H I cloud boundaries, where the steepest X-ray gradients are found.

4. MODELING

The coincidence of the $\frac{1}{4}$ keV X-ray minima with H I clouds suggests that an appreciable fraction of the X-ray emission originates on the far side of the neutral hydrogen and is absorbed by the gas of the clouds. This is qualitatively similar to observation of absorption by the distant cloud complex in Draco (Snowden et al. 1991; Burrows & Mendenhall 1991). To estimate the magnitude of the distant component, we consider a two-component model of the X-ray emission:

$$I_X = I_0 + I_1^d \times e^{-\sigma(N_H) \times N_H} . \quad (1)$$

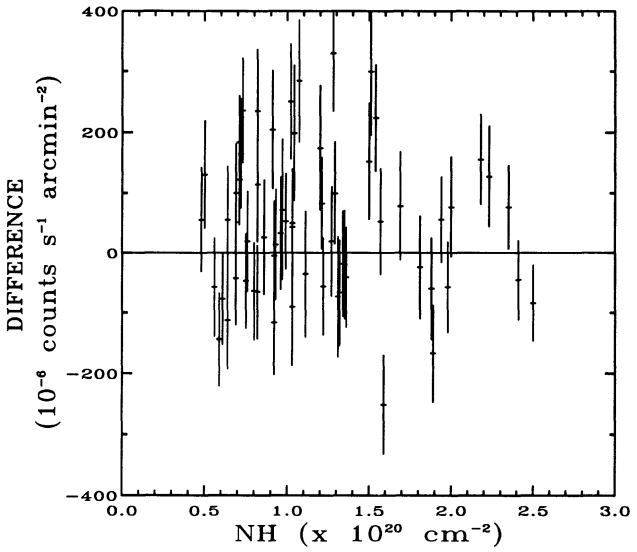

FIG. 6.—Excess $\frac{1}{4}$ keV count rate in in the 19.2 × 19.2 pixels containing Abell clusters compared to the surrounding pixels, plotted against total H I column density.

The component I_0 represents X-ray emission that is unabsorbed by the neutral gas while the component I_1^d represents X-ray emission that is absorbed by all of the neutral gas along the line of sight. The absorption cross section, $\sigma(N_H)$, is the $\frac{1}{4}$ keV band–averaged cross section derived by folding a 10^6 K thermal emission spectrum (Raymond & Smith 1977; Raymond 1988, 1991) through the Morrison & McCammon (1983) ISM absorption model and the PSPC effective area and spectral response. The value of the absorption cross section thus depends on the amount of gas, for as absorption hardens the X-ray spectrum, the effective cross section per H atom decreases (see Snowden et al. 1994b).

The X-ray data were fitted to equation (1), with I_0 and I_1^d as free parameters, by minimizing χ^2. The best-fit values are given in the first line of Table 2, along with the number of degrees of freedom and $\chi^2_{\nu-\min}$. The curve drawn through the data in Figure 5 is this fit. Errors on the coefficients are 1 σ, calculated using the criteria of Lampton, Margon, & Bowyer (1976). The fact that $\chi^2_{\nu-\min} > 2$ indicates that the model does not describe the data very well, as we would expect from the lack of detailed anticorrelation discussed qualitatively in § 3.3. Table 2 shows also that the model is not a good fit to the data even if the assumption of uniform I_0 and I_1^d across this large field is relaxed by fitting equation (1) separately for each of four quadrants of the field that meet at $(\alpha, \delta)_{2000} = (10^h16^m, 59°20')$.

Finally, we fitted each quadrant individually, and the region

TABLE 2

MODEL FITS[a]

Region	I_0 (10^{-6} counts s^{-1} arcmin^{-2})	I_1^d (10^{-6} counts s^{-1} arcmin^{-2})	ν	$\chi^2_{\nu-\min}$
Whole	695 ± 06	694 ± 25	2746	2.30
NE	662 ± 16	804 ± 50	535	1.85
SE	666 ± 22	855 ± 65	697	1.88
NW	695 ± 20	590 ± 50	644	2.24
SW	794 ± 28	510 ± 60	864	2.54

[a] Model: $I = I_0 + I_1^d \times e^{-\sigma(N_H) \times N_H}$.

as a whole, to models of the form

$$I_X = I_0 + I_1^i \times e^{-\sigma(N'_H) \times N'_H} + I_1^d \times e^{-\sigma(N_H) \times N_H}, \quad (2)$$

where N_H is the total N_H along the line of sight as before, I_1^d is the intensity of the X-ray component that is absorbed by all Galactic H I, N'_H is the column density of H I in only one of the three velocity intervals: $+25$ km s$^{-1} > V_{LSR} > -25$ km s^{-1}, -25 km s$^{-1} > V_{LSR} > -75$ km s^{-1}, or -75 km s$^{-1} > V_{LSR} > -175$ km s^{-1}, and I_1^i is the X-ray component that is absorbed by only N'_H. This model tries to incorporate into our analysis the possibility that part of the X-ray–emitting volume lies behind only one of the H I components. Variations of this model were also tried using combinations of two velocity components for N'_H. None gave a significant improvement in the fit. In sum, while the observations have the qualitative form of simple absorption, in detail this model is unsatisfactory.

5. DISCUSSION

5.1. *Problems with the Simple Model*

The X-ray and H I data displayed as maps show a striking anticorrelation which, however, is not well fitted by a simple model of uniform X-ray–emitting layers with absorption by intervening H I. Here we discuss briefly some possible reasons for this.

1. *Spatial nonuniformity of the "local" component.*—This is not likely, because although the unabsorbed Galactic component of the soft X-ray background must vary by at least a factor of 2.5 on very large angular scales (see, for example, McCammon & Sanders 1990), there is evidence that it does not change appreciably across this field. The five high-N_H features in Table 1 are located around the edges of the field, and four of them have X-ray fluxes within 1.5 σ ($\sim$5%) of 700×10^{-6} counts s^{-1} arcmin^{-2}. The lone exception, feature 4, which has $\sim$19% higher intensity than the others, may also be more transparent than the others since it is much less bright in the *IRAS* 100 μm map and may therefore have no absorption due to molecular gas. Since the X-ray flux at the deepest cloud shadows is the same on both sides of the region, it is reasonable to conclude that the foreground emission is uniform across it as well.

2. *Spatial nonuniformity of the "distant" (beyond the Galactic H I) component.*—This is likely a major factor. Figure 3 shows not only that the X-ray maxima are often displaced from the N_H minima but also that there are features in the X-rays where there are no corresponding variations in the H I column density. Identifying these variations with the "distant" rather than the "local" component follows from the observation above that the cloud shadows have a uniform minimum intensity. The variations required here would be at least a factor of 2 on scales of a few degrees.

3. *Intermixed emission and absorption.*—The emitting and absorbing material may be more interleaved than the neat layering assumed in the model. This would tend to flatten the absorption curve and make it more similar to the observed relation shown in Figure 5. No simple model of this kind will fit the data acceptably, however.

4. *Small-scale fluctuations.*—These were discussed in § 3.3. The unresolved extragalactic sources, Abell clusters, and an unexplained excess of large deviations all contribute to the excess χ^2, but the large-scale problems listed above are more important.

5. *Absorption not evaluated correctly.*—There are at least three potential pitfalls here. We have used 21 cm measurements to estimate the absorbing column densities, and while there is little ambiguity in turning the measured line profiles into H I column densities, these will not account for absorption associated with molecular or ionized hydrogen. CO emission has been observed in the two intermediate negative velocity clouds at locations 1 and 2 in Table 1, and in the low-velocity finger that extends downward from the center of the north edge of the field (Heiles et al. 1988; Reach 1993). While this means that the thickest clouds are even more opaque than would be expected from their H I column densities, it is still unlikely that there is significant molecular gas in most of this field, where N_H is $< 1.5 \times 10^{20}$ cm^{-2}. The average H II column density in the field is discussed below, but essentially nothing is known about its small-scale distribution.

Another factor is that the effective absorption cross section is quite sensitive to the assumed spectrum, since atomic cross sections change by a large factor within the energy band used here. For example, the cross section changes by 30% between a $10^{6.0}$ K and a $10^{6.2}$ K thermal spectrum and drops by 30% for either of these after it has been absorbed by 1×10^{20} H cm^{-2}. Small changes in the source spectrum in different parts of the field can therefore have a significant effect on the expected absorption (see Snowden et al. 1994b).

Taking all of the above points into consideration involves far too many free parameters to be practical, at least until the geometry of the emitters and absorbers is better understood. Distances to the H I clouds are being determined by optical interstellar absorption measurements, and *ROSAT* pointed observations of the edges of some of the clouds will allow a detailed spectral analysis of the absorption. These additional data may make more sophisticated modeling profitable. In the meantime, we turn to some interesting conclusions that can be reached with little dependence on models.

5.2. *The Extragalactic Intensity*

A very long *ROSAT* pointed exposure toward the low-N_H part of this field has been analyzed by Hasinger et al. (1993) to determine the contribution of extragalactic discrete sources. They find that resolved sources with 0.5–2 keV fluxes in the range 0.2 to 4×10^{-14} ergs cm^{-2} s^{-1} contribute 130×10^{-6} counts s^{-1} arcmin^{-2} to the $\frac{1}{4}$ keV band in a field where the average N_H is 5.3×10^{19} cm^{-2}. The $\sim$15 deg^2 of the Ursa Major survey field with $N_H < 6 \times 10^{19}$ cm^{-2} has an average $N_H = 5.5 \times 10^{19}$ cm^{-2}, and point sources have been removed to a limiting flux of approximately 14×10^{-14} ergs cm^{-2} s^{-1}. Correcting the total source flux from the deep survey to this brighter limit ($\times 1.24$) using the log N–log S relation of Hasinger et al. (1993) and for the slightly higher absorption ($\times 0.98$), gives 158×10^{-6} counts s^{-1} arcmin^{-2}, or $\sim$15% of the average diffuse intensity of 1066×10^{-6} counts s^{-1} arcmin^{-2} observed in this part of the survey field. Optical identifications of the resolved sources show that less than 10% of them are Galactic; most are identified with QSOs at $z = 1 - 2$.

Hasinger et al. (1993) find the summed spectrum of their resolved sources (with fluxes from 0.2 to 4×10^{-14} ergs cm^{-2} s^{-1}) is well fitted by the simple power-law spectrum $5.5E^{-0.96}$ keV cm^{-2} s^{-1} sr^{-1} keV^{-1}, with absorption by $8.7 \pm 2.4 \times 10^{19}$ H cm^{-2}. Correcting the coefficient by the same factor of 1.24 used above to account for the higher source flux limit in the survey data and adding the additional average column

density gives $6.9E^{-0.96}$ keV cm^{-2} s^{-1} sr^{-1} keV^{-1} absorbed by 8.9×10^{19} H cm^{-2} as the composite spectrum of the known extragalactic sources included in our "diffuse" intensity measurement.

The apparent absorption in this spectrum is somewhat larger than the 5.5×10^{19} H cm^{-2} measured H I column density, but we have not yet taken into account absorption by helium and metals associated with the diffuse H II layer. The H II layer has an *average* column density of 7×10^{19} csc b H II cm^{-2} (Reynolds 1991), so the expected column in this direction would be 8.7×10^{19} H II cm^{-2}. The $\frac{1}{4}$ keV band effective absorption cross section for normal abundances is reduced about 28% when the hydrogen is fully ionized. The ionization state of helium in the diffuse H II is unknown, but the O stars thought to ionize the hydrogen cannot produce significant double ionization of helium, and singly ionizing it reduces its cross section by only 27%. Recent models give He II/He = 0.6 (Domgörgen & Mathis 1994), while measurements of the λ5876 He recombination line give He II/He < 0.3 for one line of sight in the Galactic plane (Reynolds 1993). If we assume the helium is 50% singly ionized, the effective absorption cross section of the H II component in the $\frac{1}{4}$ keV band is 62% of that for entirely neutral gas. This would give an additional effective column density of 5.4×10^{19} H cm^{-2} on average for this Galactic latitude. One might worry that the unusually low H I column density in this direction is caused by an unusually high ionized fraction, but the observed diffuse Hα emission is actually at least a factor of 4 lower than the average for $b = 53°$, strictly limiting the H II column density to little more than the typical value, even with an assumed filling factor of unity (Reynolds 1993). The probable value implied by the Hα limit is $\lesssim 2.7 \times 10^{19}$ H cm^{-2} if the scale height and filling factor remain close to their average values. The agreement with the absorption fit to the observed spectrum is therefore very good, and while there is no reason to expect that the average QSO spectrum should not have either a soft bump or intrinsic absorption, this observation suggests that it is close to a simple power law below 2 keV. We will therefore assume in the following that the intrinsic spectrum of the extragalactic sources is an $E^{-0.96}$ power law, and that the equivalent absorbing column density of the H II layer in the UMa field is $\sim 3.4 \times 10^{19}$ H cm^{-2}.

In the 1.5 keV band (*ROSAT* bands R6 and R7), the high-latitude diffuse flux observed after removal of point sources to the 14×10^{-14} ergs cm^{-2} s^{-1} level is 120×10^{-6} counts s^{-1} arcmin^{-2} and is apparently almost entirely extragalactic. The resolved source flux is 63 in these units, or 53% of the total (Hasinger et al. 1993). If we assume that the rest of the extragalactic background has the same spectrum as these resolved sources, then we find that in the $\frac{1}{4}$ keV band, $158 \times 10^{-6}/0.53 = 298 \times 10^{-6}$ counts s^{-1} arcmin^{-2} or 28% of the observed intensity in our low-N_H region should be extragalactic. We emphasize that this field has an unusually low column density, and thus the extragalactic $\frac{1}{4}$ keV contribution would be at least a factor of 3 lower in most other high-latitude directions.

Extrapolating this to outside the 5.5×10^{19} H cm^{-2} measured Galactic H I gives 478×10^{-6} counts s^{-1} arcmin^{-2}, and the more uncertain extrapolation to outside the high-z H II layer (assumed equivalent to 3.4×10^{19} H cm^{-2}) gives 696 in these units. (We have used the average source spectrum observed by Hasinger et al. 1993 to calculate the effective cross sections.) We can use the observed log N–log S relation (Hasinger et al. 1993) to extrapolate this to infinite source flux cutoff ($\times 1.13$), and get 788×10^{-6} counts s^{-1} arcmin^{-2}, or 54 keV cm^{-2} s^{-1} sr^{-1} keV^{-1} at 0.25 keV. The actual extragalactic flux could be either greater or less than this, since the remaining 47% of the background could be either softer or harder than the 53% that is currently resolved into discrete sources. We note that this estimate is somewhat larger than an old upper limit of 45 keV cm^{-2} s^{-1} sr^{-1} keV^{-1} placed on the extragalactic intensity in the direction of the Small Magellanic Cloud (see McCammon & Sanders 1990), and that Hasinger et al. (1993) find their faintest resolved sources to be harder than the average.

5.3. *Limits on Local and Halo Intensities*

One of the most intriguing recent results in the study of the Galactic diffuse background has been the discovery by Snowden et al. (1991) and Burrows & Mendenhall (1991) that a substantial $\frac{1}{4}$ keV band intensity originates beyond the Draco nebula, an interstellar cloud that optical absorption measurements place at least 200 pc above the Galactic plane. This is the first solid evidence for 10^6 K gas in the Galactic halo, and an obvious question is whether this is a localized hot spot or part of a pervasive halo. Here, we place an upper limit on halo emission behind a small region in Ursa Major and show that it is significantly less bright than in Draco. The Draco fields are at $(l, b) = (94.^\circ7, +37.^\circ6)$ (Snowden et al. 1991) and $(89.^\circ5, +38.^\circ6)$ (Burrows & Mendenhall 1991), $\sim 41°$ away from the Ursa Major low-N_H region, which is centered near $(149.^\circ3, +53.^\circ2)$.

The halo brightness in Draco derived by Snowden et al. (1991) assumed that the halo emission originates beyond all the Galactic H I. We do not know the distances to any of the H I in Ursa Major, so to avoid ambiguity we will take the working definition of "halo" to be that it is what lies beyond all the H I, regardless of how far away the H I happens to be. We will derive an upper limit for the average halo intensity in the ~ 15 deg^2 in Ursa Major where the total column density is $< 6 \times 10^{19}$ H cm^{-2}. Other choices for the test area would in general give different limits, but the number we get here will be valid for the average halo intensity over these 15 deg^2.

The average observed X-ray intensity in this area is 1066×10^{-6} counts s^{-1} arcmin^{-2}, and we can safely subtract the 158×10^{-6} counts s^{-1} arcmin^{-2} that is resolved into extragalactic discrete sources. An upper limit involving few assumptions is obtained by dividing the remainder by the calculated transmission of the 5.5×10^{19} H cm^{-2} Galactic H I, which is 0.55 for a 10^6 K thermal spectrum. The resulting upper limit to halo emission is 1650×10^{-6} counts s^{-1} arcmin^{-2}. We compare this to the observation in Draco, where Snowden et al. (1991) fitted a two-component model and found that the intensity of the "background" component, assumed to originate beyond all the Galactic H I, was $3420 \pm 560 \times 10^{-6}$ counts s^{-1} arcmin^{-2}. (No discrete sources were excluded in their analysis.) We again subtract the flux due to the known extragalactic source population, which is $158/0.62 = 254 \times 10^{-6}$ counts s^{-1} arcmin^{-2} after correction to outside the Galactic H I. This leaves $3166 \pm 560 \times 10^{-6}$ counts s^{-1} arcmin^{-2} for the halo plus remaining extragalactic intensity. We have not made a correction for absorption by H II, since Snowden et al. (1991) did not, and it seems very unlikely that the Ursa Major field, which is at a 16° higher Galactic latitude and shows unusually low diffuse Hα emission, has a *larger* H II column density than Draco.

This already shows that there must be at least factor of ~ 2 variations in the halo emission between these two locations, but the substantial intensity remaining in the shadows of the nearly opaque H I clouds surrounding the Ursa Major field shows that a large part of the observed flux is from nearer than the H I clouds, and therefore, by our working definition, not part of the halo emission. The two-component fits to the entire field in § 4 are suspect because the assumptions of uniform foreground and background emission do not seem to be satisfied. However, the local intensity derived from the model, 695×10^{-6} counts s^{-1} arcmin^{-2} (Table 2) is in good agreement with the values observed in the deepest cloud shadows (Table 1), where the presence of molecular gas in addition to the H I probably makes them essentially opaque. (This is ~ 1.5 times the local intensity derived by both observations in Draco and is over 2.5 times the minimum $\frac{1}{4}$ keV band intensity seen in the Galactic plane.) The total rate predicted by the best-fit local and distant intensities for the $N_{\rm HI} < 6 \times 10^{19}$ H cm^{-2} region, $695 \pm 6 + 0.55 \times 694 \pm 25 = 1077 \pm 15 \times 10^{-6}$ counts s^{-1} arcmin^{-2}, is also within 1% of the average observed intensity for this region (1066×10^{-6} counts s^{-1} arcmin^{-2}).

We therefore take 683×10^{-6} counts s^{-1} arcmin^{-2} as a 2 σ lower limit to the local intensity and subtract both this and the 158×10^{-6} counts s^{-1} arcmin^{-2} due to the extragalactic point sources to get 225×10^{-6} counts s^{-1} arcmin^{-2} as an upper limit to the observed halo flux. Correcting to outside the H I layer (55% transmission for the 0.55×10^{19} H cm^{-2}, assuming 10^6 K thermal emission) gives 409×10^{-6} counts s^{-1} arcmin^{-2} as an upper limit to the intrinsic halo intensity in this direction (again uncorrected for absorption in the H II layer).

This is a factor of 7.7 smaller than the halo flux in Draco estimated by Snowden et al. (1991). This ratio could be decreased only if there were significant molecular absorption overlying the low-$N_{\rm H}$ region in Ursa Major, which seems highly unlikely at such a low total column density, or if the uniform local intensity seen in the cloud shadows around the edges of the field were to decrease near the center, at the location of the low-$N_{\rm H}$ region.

It is also interesting to make a "best" estimate of the halo intensity. To do this, we assume that the unresolved part of the 1–2 keV extragalactic diffuse background can be extrapolated to $\frac{1}{4}$ keV with the same spectrum as the 53% of it that has been resolved into sources (see § 5.2), giving 298×10^{-6} counts s^{-1} arcmin^{-2} as the observed extragalactic rate. We adopt the 695×10^{-6} counts s^{-1} arcmin^{-2} local intensity derived from the model fit to the total field, as given in Table 2. Subtracting this and the assumed extragalactic flux from the 1066×10^{-6} counts s^{-1} arcmin^{-2} total observed flux leaves only 73×10^{-6} counts s^{-1} arcmin^{-2}, or 7% of the total, as the observed halo flux. Correcting this for the 55% transmission of the Galactic H I implies 133×10^{-6} counts s^{-1} arcmin^{-2} outside the Galactic H I, or only $\sim 5\%$ of that determined by Snowden et al. (1991) in Draco (now 2940×10^{-6} counts s^{-1} arcmin^{-2} after subtracting the larger assumed extragalactic contribution).

On a smaller scale, if we interpret the intensity variations over the Ursa Major field that are not correlated with $N_{\rm H}$ as being due to variations in the halo intensity, changes of at least a factor of 2 on scales of a few degrees would be required. In Draco, Burrows & Mendenhall (1991) used only *IRAS* 100 μm data to estimate absorbing column densities, which does not allow an accurate extrapolation of the distant component to outside the Galactic H I. They have since redone the analysis with a combination of CO and H I data, and obtain a distant intensity of $2110 \pm 300 \times 10^{-6}$ counts s^{-1} arcmin^{-2} (Mendenhall 1993). After correction for the observed extragalactic sources, this gives a halo intensity of $\sim 1856 \times 10^{-6}$ counts s^{-1} arcmin^{-2}, or 58 $\pm$ 14% of that derived by Snowden et al. (1991) for their field, 4° away.

6. CONCLUSIONS

We have presented maps of a 300 deg^2 region around the very low $N_{\rm H}$ region in Ursa Major in the column density of neutral hydrogen and in the $\frac{1}{4}$ keV X-ray emission measured by the *ROSAT* all-sky survey. The maps are strikingly correlated, with pronounced X-ray minima coincident with the local $N_{\rm H}$ maxima. Conversely, the X-ray maxima are generally in directions of low $N_{\rm H}$.

An attempt to fit the X-ray data to a simple two-component model of the form $I_X = I_0 + I_1 \times \exp[-\sigma(N_{\rm H}) \times N_{\rm H}]$ does not result in an acceptable $\chi^2_{\rm min}$ value. The large value for $\chi^2_{\rm min}$ is due partly to pixel-to-pixel fluctuations in the X-ray data, but primarily to variations over angular scales $\sim 5°$. Apparently a model consisting of nearby and distant uniform regions separated by the observed H I is not valid.

The upper limit to any halo intensity originating outside the Galactic H I distribution in a 15 deg^2 field in Ursa Major is $< 409 \times 10^{-6}$ counts s^{-1} arcmin^{-2}. This is $\sim 13\%$ of the intensity inferred to originate behind the Draco nebula (Snowden et al. 1991). The observations also suggest factor of 2 fluctuations in the halo intensity on scales of several degrees in both Draco and Ursa Major. The implication is that the 10^6 K X-ray–emitting halo consists of scattered hot spots, perhaps where bubbles have broken out of the H I disk. Such spots might be nearby examples of the "wormholes" of Koo, Heiles, & Reach (1992), which they suggest are superbubbles that have broken through the Galactic H I layer.

This picture is marred by one observational problem. If we assume that many of the high-latitude $\frac{1}{4}$ keV band bright regions are due to localized halo "hot spots" showing through the Galactic H I layer, it is very difficult to explain why observations at lower energies, where the absorption cross sections are much larger, usually show very nearly the same amount of brightening. For example, the Draco nebula is located near one edge of a bright $\frac{1}{4}$ keV band feature $\sim 15°$ across (cf. McCammon et al. 1983; Snowden et al. 1994a). It is tempting to associate this with the apparently bright halo emission behind the nebula (Hirth et al. 1985). However, the feature would be seen through a column density of $\sim 1 \times 10^{20}$ H cm^{-2} or more, while its C/B band intensity ratio (derived from McCammon et al. 1983) is within 5% of that seen in the Galactic plane below the enhancement, where the total intensity is 3.4 times smaller. Since the effective absorption cross section for the B band ($\sim$130–188 eV) is twice that for the C band ($\sim$160–284 eV), this requires that the intrinsic halo emission be much softer: at just the right temperature to look the same after absorption as the spectrum in the Galactic plane. The problem is compounded by observations in the yet softer Be band ($\sim$70–111 eV), where the effective cross section is ~ 6 times larger than in the B band. There is not a good Be band observation of this particular feature, but for the $\sim 17\%$ of the sky that has been observed, the Be/B band ratio is essentially constant within the $\sim 15\%$ statistical accuracy of the measurements over a range of a factor of 3 in intensity (Bloch et al. 1986; Juda et al. 1991). A general discussion of this problem

can be found elsewhere (Snowden et al. 1990; McCammon & Sanders 1990).

Additional *ROSAT* observations of intermediate- and high-latitude interstellar clouds whose distances have been or will be determined by optical interstellar absorption measurements should enable considerable progress to be made in solving this long-standing problem. Many suitable *ROSAT* observations have already been made, but much additional optical work is needed for distance determinations.

This research was supported in part by the National Aeronautics and Space Administration under grants NAG 5-679, NAG 5-1726, and NAG 5-1817 and by the Max-Planck Institute for Extraterrestrial Physics.

REFERENCES

Albert, C. E. 1983, ApJ, 272, 509
Albert, C. E., Blades, J. C., Morton, D. C., Lockman, F. J., Proulx, M., & Ferrarese, L. 1993, ApJS, 88, 81
Aschenbach, B. 1988, Appl. Opt., 27 (8), 1404
Bloch, J. J., Jahoda, K., Juda, M., McCammon, D., Sanders, W. T., & Snowden, S. L. 1986, ApJ, 308, L59
Bregman, J. N. 1980, ApJ, 236, 577
Burrows, D. N., Kraushaar, W. L., McCammon, D., & Sanders, W. T. 1984, ApJ, 287, 208
Burrows, D. N., & Mendenhall, J. A. 1991, Nature, 351, 629
Chevalier, R. A., & Oegerle, W. R. 1979, ApJ, 227, 398
Danly, L. 1989, ApJ, 342, 785
Domgörgen, H., & Mathis, J. S. 1994, ApJ, 428, 647
Edgar, R. J., & Chevalier, R. A. 1986, ApJ, 310, L27
Goerigk, W., Mebold, U., Reif, K., Kalberla, P. M. W., & Velden, L. 1983, A&A, 120, 63
Hasinger, G., Burg, R., Giacconi, R., Hartner, G., Schmidt, M., Trümper, J., & Zamorani, G. 1993, A&A, 275, 1
Heiles, C., Reach, W. T., & Koo, B.-C. 1988, ApJ, 332, 313
Hirth, W., Mebold, U., & Müller, P. 1985, A&A, 153, 249
Jahoda, K., Lockman, F. J., & McCammon, D. 1990, ApJ, 354, 184
Juda, M., Bloch, J. J., Edwards, B. C., McCammon, D., Sanders, W. T., Snowden, S. L., & Zhang, J. 1991, ApJ, 367, 182
Koo, B.-C., Heiles, C., & Reach, W. T. 1992, ApJ, 390, 108
Lampton, M., Margon, B., & Bowyer, S. 1976, ApJ, 208, 177
Lilienthal, D., Wennmacher, A., Herbstmeier, U., & Mebold, U. 1991, A&A, 250, 150
Lockman, F. J. 1991, in IAU Symp. 144, The Interstellar Disk-Halo Connection in Galaxies, ed. H. Bloemen (Dordrecht: Kluwer), 15
Lockman, F. J., Jahoda, K., & McCammon, D. 1986, ApJ, 302, 432
Marshall, F. J., & Clark, G. W. 1984, ApJ, 287, 633
McCammon, D., Burrows, D. N., Sanders, W. T., & Kraushaar, W. L. 1983, ApJ, 269, 107
McCammon, D., Meyer, S. S., Sanders, W. T., & Williamson, F. O. 1976, ApJ, 209, 46
McCammon, D., & Sanders, W. T. 1990, ARA&A, 28, 657
Mebold, U., Cernicharo, J., Velden, L., Reif, K., Crezalius, C., & Goerigk, W. 1985, A&A, 151, 427
Mendenhall, J. A. 1993, private communication
Morrison, R., & McCammon, D. 1983, ApJ, 270, 119
Odenwald, S. F., & Rickard, L. J. 1987, ApJ, 318, 702
Pfeffermann, E., et al. 1987, Proc. SPIE, 733, 519
Plucinsky, P. P., Snowden, S. L., Briel, U. G., Hasinger, G., & Pfeffermann, E. 1993, ApJ, 418, 519
Raymond, J. C. 1988, in Hot Thin Plasmas in Astrophysics, ed. R. Pallavicini (Dordrecht: Kluwer), 3
———. 1991, private communication, computer code update
———. 1992, ApJ, 384, 502
Raymond, J. C., & Smith, B. W. 1977, ApJS, 35, 419
Reach, W. T. 1993, ApJ, submitted
Reynolds, R. J. 1991, in IAU Symp. 144, The Interstellar Disk-Halo Connection in Galaxies, ed. H. Bloemen (Dordrecht: Kluwer), 67
———. 1993, private communication
Shapiro, P. R., & Field, G. B. 1976, ApJ, 205, 762
Snowden, S. L., et al. 1994a, in preparation
Snowden, S. L., Cox, D. P., McCammon, D., & Sanders, W. T. 1990, ApJ, 354, 211
Snowden, S. L., & Freyberg, M. J. 1993, ApJ, 404, 403
Snowden, S. L., McCammon, D., Burrows, D. N., & Mendenhall, J. A. 1994b, ApJ, 424, 714
Snowden, S. L., Mebold, U., Hirth, W., Herbstmeier, U., & Schmitt, J. H. M. M. 1991, Science, 252, 1529
Snowden, S. L., Plucinsky, P. P., Briel, U., Hasinger, G., & Pfeffermann, E. 1992, ApJ, 393, 819
Snowden, S. L., & Schmitt, J. H. M. M. 1990, Ap&SS, 171, 207
Spitzer, L. 1956, ApJ, 124, 20
Stark, A. A., Gammie, C. F., Wilson, R. W., Bally, J., Linke, R. A., Heiles, C., & Hurwitz, M. 1992, ApJS, 78, 77
Trümper, J. 1983, Adv. Space Res., 2(4), 241
Voges, W. 1992, in Proc. of the European International Space Year Conference, ESA ISY 3, ed. T. D. Guyenne & J. J. Hunt (Noordwijk: ESA), 9
Voges, W., et al. 1992, in Proc. of the European International Space Year Conference, ESA ISY 3, ed. T. D. Guyenne & J. J. Hunt (Noordwijk: ESA), 223

Note added in proof.—We have received a preprint (R. A. Benjamin, K. A. Venn, C. Sneden, & D. D. Hiltgen, 1994) that reports that the distance of one of the intermediate-velocity clouds in this Ursa Major field (G153.5 + 51.3) is at least 240 pc and may be as great as 410 pc.

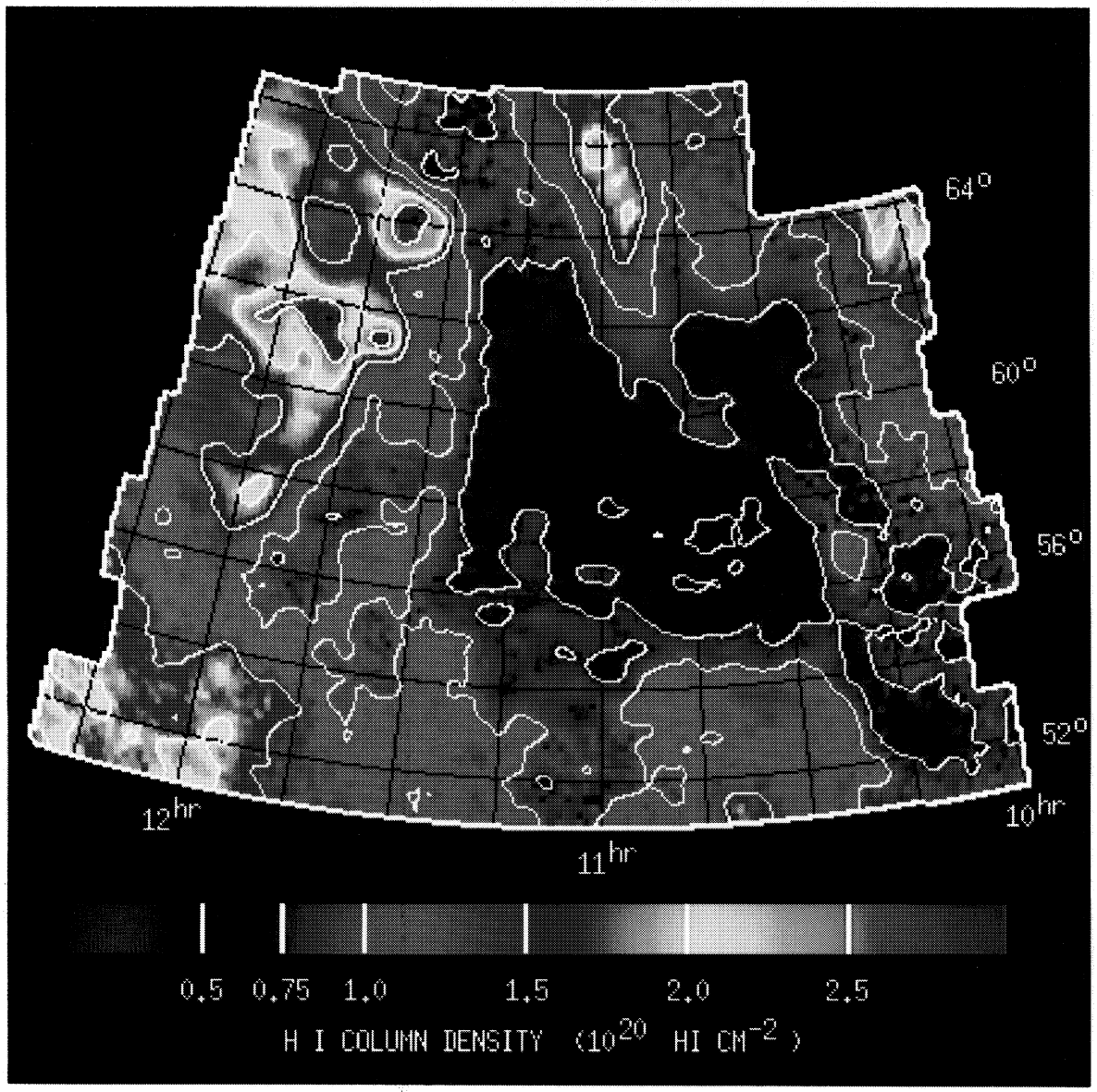

FIG. 2.—Total H I column density, N_H, for the Ursa Major field. Coordinates are J2000. Contours are drawn at 0.5, 0.75, 1.0, 1.5, 2.0, and 2.5 × 10^{20} cm^{-2}.

SNOWDEN et al. (see 430, 603)

PLATE 32

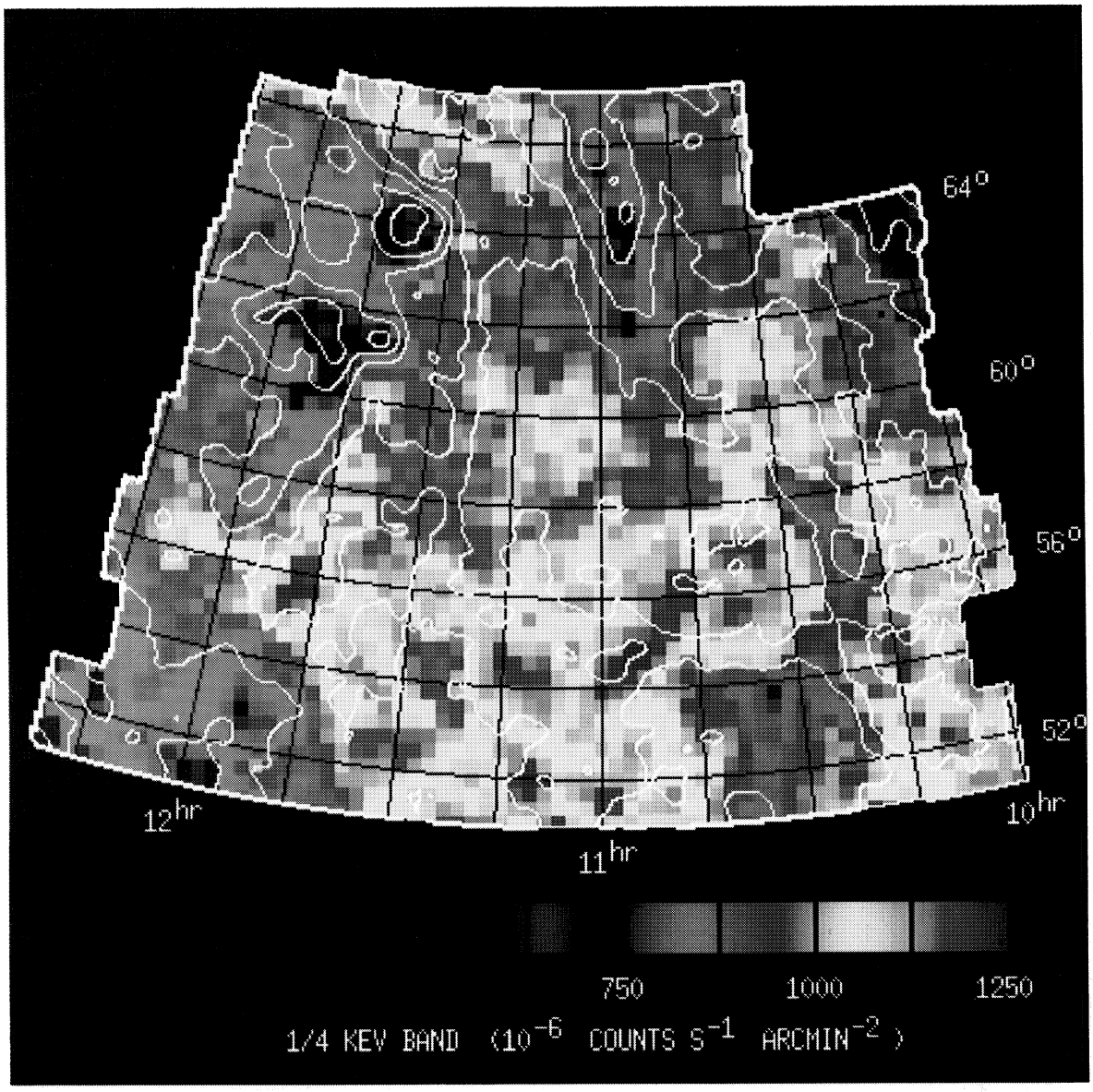

FIG. 3.—$\frac{1}{4}$ keV band map of X-ray emission (color levels) with superposed H I column density contours. Coordinates are J2000. Contours are the same H I contours shown in Fig. 2. The color bar at the bottom of the figure gives the X-ray count rates in units of 10^{-6} counts s^{-1} arcmin^{-2}.